The Design and Construction of Two Experimental Setups to Measure Thermoelectric Properties of Novel Materials

by

Steven A. Moses

A thesis submitted in partial fulfillment
of the requirements for the degree of
Bachelor of Science, Honors
(Physics)
at the University of Michigan
2010

Research Advisor:

Prof. Ctirad Uher, Professor of Physics

ACKNOWLEDGEMENTS

There are many people I would like to thank who have helped and assisted me during my undergraduate career. Prof. Ctirad Uher has taught and mentored me since I entered the university. After taking Honors Physics I with him my first semester, he gave me the opportunity to work in his lab, starting the second semester of my freshman year. Since then, he has guided me and advised me about the project which is the subject of this thesis, and about physics in general. Working in his lab gave me many other opportunities, and helped me win several scholarships and get accepted to several summer internships.

Next, I would like to thank the other people in the lab who I worked with on a daily basis: Dr. Xun Shi, Dr. Huijun Kong, Dr. Changpeng Li, Dr. Guoyu Wang, and Sedat Ballikaya. I would also like to thank the other undergraduates who worked in the lab, including Derek Vermeulen, Jason Ball, and Drake Austin.

Finally, I would like to thank all of the other teachers and mentors who have helped me along the way: Prof. Jean Krisch, Prof. Georg Raithel, Prof. James Thompson, Prof. Gerry Gabrielse, Dr. Jonathan Wrubel, Prof. Homer Neal, Prof. Aaron Leanhardt, Prof. Tim McKay, Dr. Elleanor Crown, and many others.

I would like to thank several collaborators at other universities who are responsible for some of the data and analysis presented in this thesis, namely the group of Prof. Mercouri Kanatzidis at Northwestern University.

This work was funded by MURI program, which is sponsored by the Office of

Naval Research, and the National Science Foundation (for funding my REU stipend during summer 2007).

TABLE OF CONTENTS

LIST OF FIGURES

Figure

ABSTRACT

Two experiments to measure properties of thermoelectric materials at high temperature were designed, constructed, and are currently being operated. One measures the Hall coefficient at high temperature, while the other measures electrical conductivity. Measuring the Hall coefficient allows for the determination of the carrier density in the material and allows for the calculation of electron and hole mobility. The conductivity experiment utilizes an AC measurement, and a LabVIEW VI was written to automate the acquisition of data. After describing the experiments in considerable detail, data is presented and the relationship of the Hall coefficient and conductivity to other other thermoelectric properties is discussed.

CHAPTER I

Introduction

The study of thermoelectric materials is a very active area of modern research that combines aspects of physical chemistry, solid state physics, and materials science. A thermoelectric material is a material that converts heat to electricity and electricity to heat. The main motivation for studying thermoelectrics is to find ways to improve their performance to better implement them in practical systems.

Most industrial processes waste a significant fraction of the input energy by producing waste heat. If efficient thermoelectric materials could be developed, they could be used to convert waste heat to electricity in automobile exhaust systems and other industrial processes. This could reduce the wasted energy in such processes by 10% or more [1], which would significantly reduce energy consumption. In the case of an automobile, if some of the heat from the exhaust system could be converted to electricity, the car would be more fuel efficient, or in the case of hybrid cars, batteries could be recharged. Two major concerns in today's society are a decreasing supply of fuels and an increase in pollution. Efficient thermoelectric materials could help to solve both of these problems.

Based on theoretical considerations, materials are developed which are thought to have good thermoelectric properties. Typically, several similar materials are devel-

oped, which differ only in the concentration of a particular dopant. Daily activities in the lab include synthesis of materials and a comprehensive measurement of the thermoelectric properties of interest. My work in the last several years has focused on improving these measurements. Two new experimental setups have been designed and tested. One enables the Hall coefficient to be measured from room temperature to 800 K (Previously, the Hall coefficient could only be measured from 4 K to room temperature). The other is an experiment which measures electrical conductivity using an AC measurement. This setup was created mainly to verify that measurements made on another experimental setup in the lab are correct.

The outline of this thesis is as follows. Chapter 2 gives a brief introduction to the theory of thermoelectric materials, with particular emphasis on those properties which will be discussed in subsequent chapters. Chapter 3 describes the high temperature Hall effect experiment. The experimental setup is described in substantial detail, and some experimental results are presented. Chapter 4 describes the high temperature conductivity experiment that was built to supplement existing experiments in the lab. A substantial portion of this project involved writing a LabVIEW VI to automate the data acquisition. A description of the experimental setup is given, and then the new system is compared to the old one. Chapter 5 gives some concluding remarks and gives an outlook for future work to be done in the field of thermoelectrics.

CHAPTER II

Fundamental Principles of Thermoelectrics

In this chapter, the main thermoelectric properties are introduced, and some theoretical results are presented that predict the values of these properties. While most of this thesis will focus on the Hall coefficient and electrical conductivity, the Seebeck coefficient and figure of merit are such fundamental properties of thermoelectrics that they will also be discussed here. Most of the derivations in the first three sections of this chapter are taken from Refs. [2] and [3].

2.1 Seebeck, Peltier, and Thomson Effects

There are three main thermoelectric effects: the Seebeck, Peltier, and Thomson effects. If a temperature gradient is applied across a junction between two materials, a voltage will develop across the junction, with the voltage related to the temperature gradient by the Seebeck coefficient. The Seebeck effect is responsible for the operation of a thermocouple. Figure 2.1 shows two different conductors, one labeled A and the other labeled B, connected as a thermocouple. There exists a temperature difference between the two ends. The Seebeck coefficient of the thermocouple is defined as

$$\alpha_{AB} = \frac{dV}{dT} \tag{2.1}$$

where V is the voltage between points x and y [3].

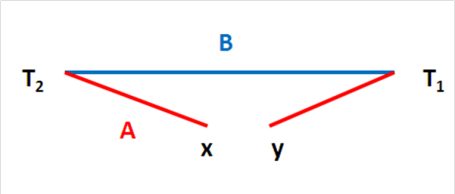

Figure 2.1: A thermocouple made out of two different materials A and B. Based on a diagram from Ref. [3].

In the case of the thermocouple in figure 2.1, $\Delta T = T_2 - T_1$. Then,

$$V_{xy} = \alpha_{AB} \Delta T \tag{2.2}$$

If T_2 is fixed and α_{AB} is known, then by measuring V_{xy}, one can determine T_1.

The Peltier effect is an effect whereby heat is liberated or absorbed at the junction between two materials in which a current is flowing through them. The heat liberated (or absorbed) at the junction is given by

$$Q = \Pi_{AB} I \tag{2.3}$$

where Π_{AB} is the Peltier coefficient [3].

If there is a temperature gradient across a material and a current is flowing through the material, then heat will be liberated or absorbed. This is the Thomson effect, and it is described by the following equation:

$$\frac{dQ}{dx} = \tau I \frac{dT}{dx} \tag{2.4}$$

where τ is the Thomson coefficient [3]. The following relationships hold for two materials A and B [3]:

$$\tau_A - \tau_B = T \frac{d\alpha_{AB}}{dT} \tag{2.5}$$

$$\Pi_{AB} = \alpha_{AB} T \tag{2.6}$$

The coefficients α_{AB} and Π_{AB} defined above are for a system consisting of two different materials with a junction between them. However, it is often useful to define absolute thermoelectric coefficients which describe a single material. All of the above equations generalize when a single material is being discussed [3]. If a material is subjected to a heat gradient ΔT, then $\Delta V = \alpha \Delta T$, where α is the Seebeck coefficient of the material. Relations (2.5) and (2.6) also apply to absolute thermoelectric coefficients, i.e. $\tau = T d\alpha/dT$ and $\Pi = \alpha T$ [3].

2.2 Figure of Merit

In order to characterize thermoelectric materials, the most important parameter is the figure of merit. Figure 2.2 shows a standard thermoelectric circuit used for an analysis of the figure of merit. The derivation presented here is taken from Refs. [2] and [3].

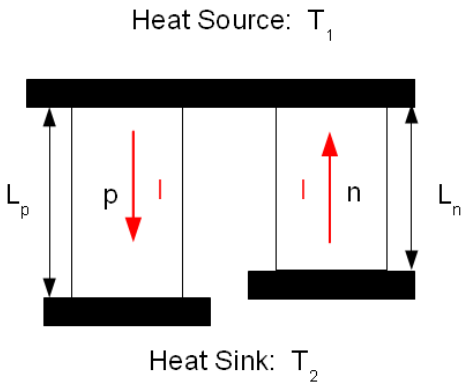

Figure 2.2: Thermoelectric refrigerator. Based on a diagram in Ref. [2].

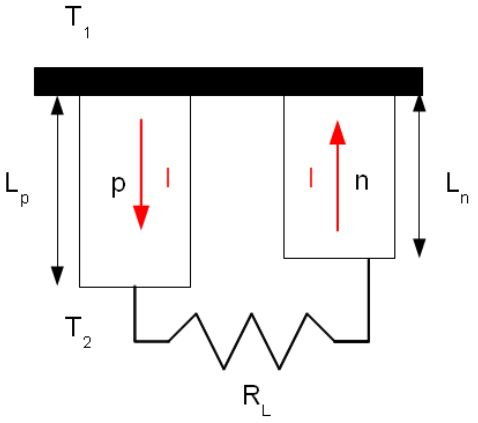

Figure 2.3: Thermoelectric generator. Based on a diagram in Ref. [2].

The circuit has a heat source at temperature T_1 and a heat sink at temperature T_2. There are two thermoelectric materials that complete the circuit, one a p-type material and the other n-type. The cross-sectional areas are A_p and A_n, respectively.

A current I flows through the circuit. Since there is a heat gradient along each branch, heat will be liberated or absorbed in each of the branches by the Peltier effect, and there will also be heat lost from thermal conduction. The heat from the source to the sink in the two branches is given by [2]:

$$q_p = \Pi_p I - \lambda_p A_p \frac{dT}{dx} = \alpha_p IT - \lambda_p A_p \frac{dT}{dx} \tag{2.7}$$

$$q_n = -\Pi_n I - \lambda_n A_n \frac{dT}{dx} = -\alpha_n IT - \lambda_n A_n \frac{dT}{dx} \tag{2.8}$$

where x is measured along the length of the sample from source to sink (see figure 2.2).

The resistance of the sample will generate heat per unit length $I^2\rho/A$. In a steady state situation, the heat gradient must be nonuniform to balance the Joule heating [2]. This means that

$$-\lambda_{p,n} A_{p,n} \frac{d^2T}{dx^2} = \frac{I^2 \rho_{p,n}}{A_{p,n}} \tag{2.9}$$

which holds separately for the p and n branches (note that equation (2.9) is actually two equations) [2]. Equation (2.9) can be integrated to give the temperature as a function of position. The boundary conditions are $T(0) = T_1$ and $T(L_p) = T(L_n) = T_2$ [2], which gives

$$\lambda_{p,n} A_{p,n} T = \frac{I^2 \rho_{p,n}(L_{p,n} x - x^2)}{2A_{p,n}} + \frac{\lambda_{p,n} A_{p,n}(T_2 - T_1)x}{L_{p,n}} + \lambda_{p,n} A_{p,n} T_1 \tag{2.10}$$

$$\lambda_{p,n} A_{p,n} \frac{dT}{dx} = -\frac{I^2 \rho_{p,n}(x - L_{p,n}/2)}{2A_{p,n}} + \frac{\lambda_{p,n} A_{p,n}(T_2 - T_1)}{L_{p,n}} \tag{2.11}$$

The cooling power q_c is given by

$$q_c = (q_p + q_n)|_{x=0} = (\alpha_p - \alpha_n)IT - K(T_2 - T_1) - \frac{I^2 R}{2} \tag{2.12}$$

where K is the thermal conductivity of the two branches in parallel and R is the resitivity of the two branches in series [2, 3].

$$K = \frac{\lambda_p A_p}{L_p} + \frac{\lambda_n A_n}{L_n} \tag{2.13}$$

$$R = \frac{L_p \rho_p}{A_p} + \frac{L_n \rho_n}{A_n} \tag{2.14}$$

Equation (2.12) shows that if q_c is considered to be a function of I, then because the third term is negative and proportional to I^2 while the first term is only proportional to I, there should be some value of the current for which q_c is maximum [2]. This current $I_{\max}$ can be found by setting $\frac{dq_c}{dI} = 0$. The results are [2]:

$$I_{\max} = \frac{(\alpha_p - \alpha_n)T_1}{R} \tag{2.15}$$

$$(q_c)_{\max} = \frac{(\alpha_p - \alpha_n)^2 T_1^2}{2R} - K(T_2 - T_1) \tag{2.16}$$

As $T_2 - T_1$ becomes larger, equation (2.16) shows that $(q_c)_{\max}$ will go to zero [2]. Thus

$$(T_2 - T_1) \leq \frac{(\alpha_p - \alpha_n)^2 T_1^2}{2KR} \tag{2.17}$$

The figure of merit Z is related to the maximum temperature difference that can be achieved. It is defined as [2]:

$$Z = \frac{(\alpha_p - \alpha_n)^2}{KR} \tag{2.18}$$

Then equation (2.17) becomes

$$(T_2 - T_1) \leq \frac{1}{2} Z T_1^2 \tag{2.19}$$

For a single material,

$$Z = \frac{\alpha^2}{\rho\lambda} = \frac{\alpha^2 \sigma}{\lambda} \tag{2.20}$$

where ρ is the resistivity, σ is the electrical conductivity, and λ is the thermal conductivity [2].

Z has units 1/temperature; a more commonly used parameter is the dimensionless figure of merit ZT, where T is the average temperature [2,3]. The expression for the figure of merit matches intuition very well–in a good thermoelectric material, the voltage produced when a heat gradient is applied should be large, i.e. it should have a high Seebeck coefficient, and the material should not conduct heat very well, i.e. it should have a low thermal conductivity. Both of these statements are correct, as can be seen by looking at the expression for Z in equation (2.20).

2.3 Performance of Thermoelectric Refrigerators and Generators

The coefficient of performance ϕ of the circuit considered in the last section (which is a refrigerator) is given by q_c/W, where W is the electrical power supplied. Electrical power must be supplied to counter both Joule heating and the Seebeck voltage [2]. The power that must be supplied to the p branch is [2]

$$W_p = \alpha_p I(T_2 - T_1) + \frac{I^2 \rho_p L_p}{A_p} \tag{2.21}$$

while the power that must be supplied to the n branch is [2]

$$W_n = -\alpha_n I(T_2 - T_1) + \frac{I^2 \rho_n L_n}{A_n} \tag{2.22}$$

Thus, it follows that [2]

$$\phi = \frac{q_c}{W_p + W_n} = \frac{(\alpha_p - \alpha_n) I T_1 - \frac{I^2 R}{2} - K(T_2 - T_1)}{I(\alpha_p - \alpha_n)(T_2 - T_1) + I^2 R} \tag{2.23}$$

By setting $d\phi/dI = 0$, one can solve for the current $I_{\max}$ that yields the maximum coefficient of performance $\phi_{\max}$. Ref. [2] shows that $I_{\max}$ and $\phi_{\max}$ are given by the

following expressions.

$$I_{\max} = \frac{(\alpha_p - \alpha_n)(T_2 - T_1)}{R\left(-1 + \sqrt{1 + \frac{Z(T_1+T_2)}{2}}\right)} \tag{2.24}$$

$$\phi_{\max} = \frac{T_1\sqrt{1 + \frac{Z(T_1+T_2)}{2}} - T_2}{(T_2 - T_1)\left(1 + \sqrt{1 + \frac{Z(T_1+T_2)}{2}}\right)} \tag{2.25}$$

Equations (2.24) and (2.25) both involve the figure of merit. Now consider what happens if a load of resistance R_{load} is connected to the circuit (see figure 2.3). This creates a generator, and the emf produced is just the Seebeck voltage [2].

$$V = (\alpha_p - \alpha_n)(T_1 - T_2) \tag{2.26}$$

The power given to the load is [2]

$$W_{\text{load}} = \left(\frac{V}{R + R_{\text{load}}}\right)^2 R_{\text{load}} = \left(\frac{(\alpha_p - \alpha_n)(T_1 - T_2)}{R + R_{\text{load}}}\right)^2 R_{\text{load}} \tag{2.27}$$

The total power dissipated in the circuit is [2]

$$Q = K(T_1 - T_2) + (\alpha_p - \alpha_n)IT_1 - \frac{I^2R}{2} \tag{2.28}$$

and the efficiency $\eta = W/Q$. It can be shown that the efficiency is related to the figure of merit in the following way [2]:

$$\eta = \frac{T_1 - T_2}{T_2} \cdot \frac{M - 1}{M + \frac{T_2}{T_1}} \tag{2.29}$$

where $M = \sqrt{1 + Z(T_1 + T_2)/2}$. Notice that the first factor in equation (2.29), $(T_1 - T_2)/T_1$, is the ideal Carnot thermodynamic efficiency. In the limit that M gets very large (which occurs when Z becomes very large), the efficiency approaches the ideal thermodynamic limit. For most good thermoelectrics, $Z(T_1 + T_2)/2 \approx 1$, so for $T_1/T_2 \approx 1$, the efficiency is about 20% of the thermodynamic limit [2]. It is clear from equation (2.29) that the figure of merit plays an important role in determining the performance of a material.

2.4 The Hall Effect

The Hall effect is a phenomenon that occurs when a conductor is placed in a magnetic field. Charge carriers in the conductor are deflected in a direction perpendicular to both the current and magnetic field. As a result, charges builds up on one side of the conductor, and a potential difference develops to compensate for this accumulated charge. One way to characterize the Hall effect in a material is to introduce a parameter known as the Hall coefficient. The Hall effect discriminates whether electrons or holes are the majority carrier in a material. It can also be used to estimate the carrier density in a material and, along with a measurement of the electrical conductivity, can be used to determine the mobility of charge carriers.

Figure 2.4 shows a basic layout of the Hall effect experiment. A conductor carries a current in the $+x$ direction, and a uniform magnetic field is applied in the $+z$ direction. If the charge carriers are electrons, then they travel in the $-x$ direction, and the Lorentz force on them will be in the $-y$ direction. The front face of the conductor (labeled A in the figure) will develop a net negative charge, and to balance this, a potential difference will develop with $V_2 > V_1$. If the charge carriers are positive, they will travel in the $+x$ direction, and the Lorentz force on them will also be in the $-y$ direction. In this case, a potential difference develops with $V_1 > V_2$. Thus, the Hall voltage $V_H = V_2 - V_1$ has a different polarity for positive and negative charge carriers, and can be used to determine the polarity of the charge carriers in the material.

The Hall coefficient R_H is defined as the ratio of the electric field in the y direction to the product of the current density j_x in the x direction and the magnetic field B_z

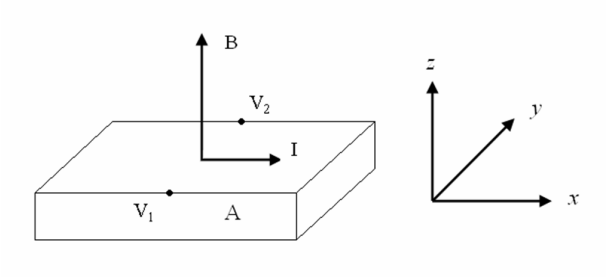

Figure 2.4: A schematic of the Hall effect

in the z direction [4].

$$R_H = \frac{E_y}{j_x B_z} \tag{2.30}$$

If the current through the conductor is I, and the sample has length l, width w, and thickness t (thickness measured along the z direction), then R_H can be expressed in the following way:

$$R_H = \frac{E_y}{j_x B} = \frac{V_H/w}{\frac{I}{wt}B} = \frac{V_H wt}{IwB} = \frac{V_H t}{IB} \tag{2.31}$$

The quantities V_H, t, I, and B are all easily measurable quantities; thus, the Hall coefficient can be computed from experimentally measured quantities. The Hall coefficient is positive when the charge carriers are positive and negative when the charge carriers are negative. It can be shown that when the carriers are all of one type, then the magnitude of the Hall coefficient is given by

$$R_H = \frac{1}{ne} \tag{2.32}$$

where n is the density of charge carriers and e is the magnitude of the fundamental charge [4]. It should be noted that in certain cases (for example, when the conductor is nondegenerate and the relaxation time depends on the energy) that equation (2.32) is not exactly correct and should be replaced by the following expression:

$$R_H = \frac{A}{ne} \tag{2.33}$$

where A is a constant slightly different from unity that depends on the dominant scattering mechanism in the material (for many nondegenerate conductors, $A = 3\pi/8$) [3].

The Hall effect can be observed in all conductors; however, it is much easier to observe in semiconductors than it is in good conductors like copper. An inspection of equation (2.32) shows why the Hall effect is hard to measure in copper. Because copper is a very good conductor, the density of electrons n is very large, which makes R_H and V_H quite small.

It is now useful to introduce the mobility, which is defined to be the magnitude of the drift velocity of charge carriers divided by the electric field [4].

$$\mu = \frac{|v|}{E} \tag{2.34}$$

If both positive and negative carriers are present in a material, then

$$R_H = \frac{\mu_h^2 p - \mu_e^2 n}{e(\mu_h p + \mu_e n)^2} \tag{2.35}$$

where μ_h and μ_e are the mobilities of holes and electrons, respectively [5]. In general, $\mu_e > \mu_h$, so that the Hall coefficient will only change sign for a p-type material [5]. The electrical conductivity can be expressed as

$$\sigma = ne\mu_e + pe\mu_h \tag{2.36}$$

where n is the concentration of electrons and p is the concentration of holes [4]. If only one carrier type is present (for here, assume only electrons are present), then equation (2.36) reduces to

$$\sigma = ne\mu \tag{2.37}$$

Equation (2.37) combined with equation (2.32) then gives

$$\mu = |R_H|\sigma \tag{2.38}$$

where the absolute value is included because the mobility is defined to be positive for all materials.

In subsequent sections, it will be assumed that there is a simple parabolic energy band and only a single type of charge carrier, so that equations (2.32) and (2.38) describe the materials of interest. In this case, the mobility can be very easily calculated from R_H and σ, which are measured experimentally.

CHAPTER III

High Temperature Hall Effect Experiment

3.1 Motivation

While the figure of merit ZT (equation (2.20)) does not directly involve the Hall coefficient, it is still useful to determine the Hall coefficient. The Hall coefficient provides a very easy way to determine the dominant charge carriers in a material (and thus determine whether the material is p-type or n-type), and it allows for the determination of the carrier concentration. The carrier concentration can be used to calculate the mobility. Overall, knowledge of the Hall coefficient helps to give a more complete understanding of the properties of a material.

Before I came to the lab, there was an experiment to measure the Hall coefficient from about 4 K to around room temperature, but it was desired to increase the range of the measurement to about 800 K. One main reason for this is that other thermoelectric properties such as electrical conductivity and the Seebeck coefficient are measured to around 700 or 800 K, and it is desirable to have Hall coefficient data in the same temperature range.

3.2 Experimental Setup

A picture of the experimental setup can be seen in figure 3.1. The three main components are the cryostat and sample mount, the furnace and temperature controller,

and the superconducting magnet.

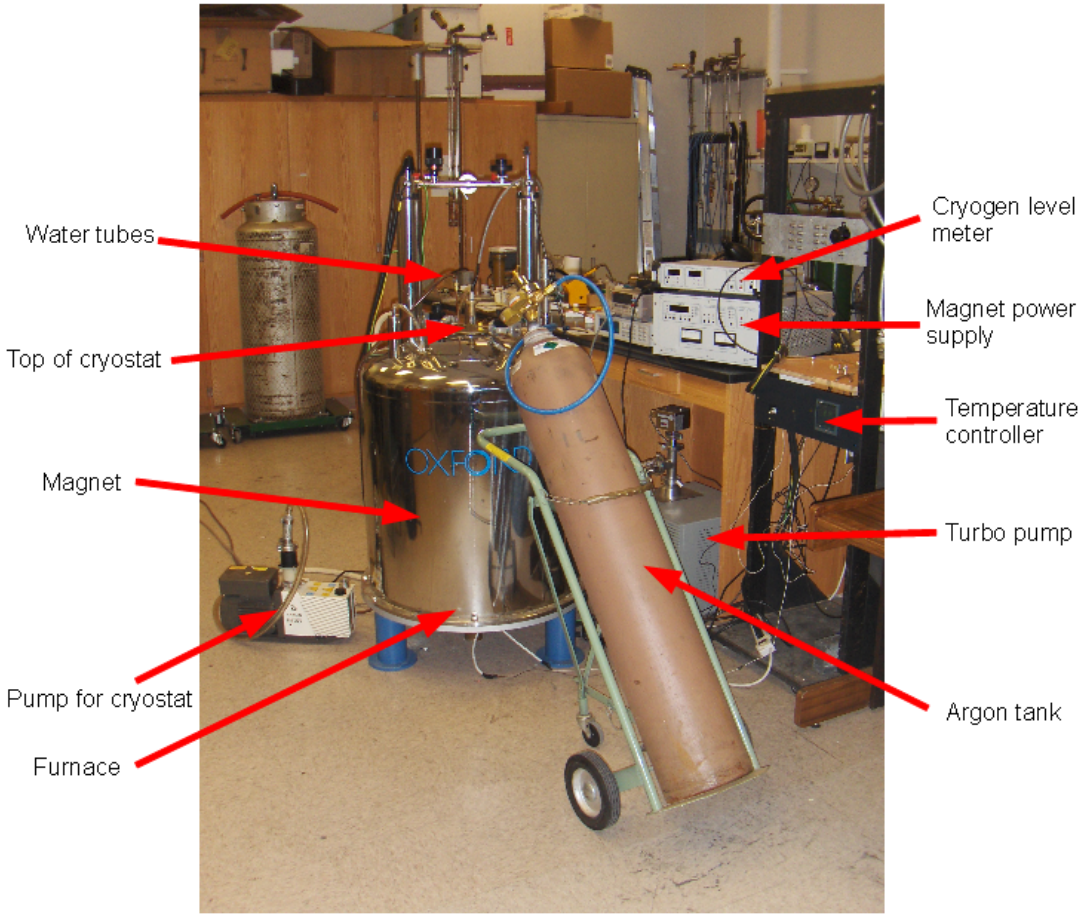

Figure 3.1: The experimental setup for both the Hall effect experiment and the conductivity experiment

A strong magnetic field is necessary to measure the Hall coefficient well. The field should be stable and approximately homogeneous over the area of the sample. There is a superconducting magnet in the lab that has a cylindrical bore about 8 cm in diameter. This magnet provides an ideal location for carrying out the high temperature Hall effect experiment. The magnet was built by Oxford Instruments, and the specifications indicate that the maximum of the field is homogeneous to 1 part

in 1000 over a volume of 1 cm^3 [6]. The samples that are measured are rectangular and about 10 mm long, 1-3 mm wide, and 1-2 mm thick, so the specified stability is sufficient for our purposes. The maximum field at which this magnet can operate is around 9 Tesla [6], although in our experiments, the magnet is usually operated at around 1 Tesla. The maximum suggested ramp rate of the magnetic field is about 0.93 Tesla/minute. Because the polarity of the magnetic field must frequently be changed during an experiment, the magnet is not operated in superconducting mode. As a result, the magnitude of the field must be frequently ramped from zero to a maximum and then back. The field at which the experiment is operated is chosen to be a compromise between reaching the desired field as quickly as possible and producing a strong enough field to make an accurate measurement.

The measurements are taken using an AC resistance bridge (Linear Research model 700). The resistance bridge sends an AC current into the sample and reads an AC voltage across the sample. It then time averages the ratio of the voltage readings to the current readings, yielding a resistance. An AC measurement has several advantages over a DC measurement [7]. When measuring resistance, current is injected into the sample; as a result of the Peltier effect, heat is absorbed at one junction between the sample and electrical contact and liberated at the opposite junction. This creates a Seebeck voltage across the sample. This Seebeck voltage would lead to an error in the measurement, but the errors cancel out for an AC measurement when averaged over a complete cycle. Heating of a junction is suppressed by reversing the current, which would then cause the junction to cool. Any other offsets would similarly average to zero. In addition, filtering the AC measurement during amplification makes the AC measurement much more sensitive than a DC measurement. Essentially, the AC measurement allows one to extract a very small

signal from a noisy background [7].

The resistance is measured using both polarities of the magnetic field (the sample is oriented horizontally; thus, the magnetic field is either vertically up or vertically down). A source of offset is a misalignment of the points used for measuring the Hall voltage (the points labeled V_1 and V_2 in figure 2.4). If these points are not exactly across from one another, there will be a voltage between them when current is flowing due to the resistivity of the sample, even if there is no magnetic field. By measuring at both polarities of the field, the error in the measurement with one polarity of magnetic field is essentially cancelled by the error in the measurement at the other polarity. To extract the Hall coefficient, the following prescription is used:

$$R_H = \frac{(R_+ - R_-)t}{2B} \tag{3.1}$$

where R_+ is the resistance reading at positive field, R_- is the resistance reading at negative field, t is the thickness of the sample, and B is the magnetic field. One can verify that the above expression has the proper units (m^3/C). Also, writing $R_+ - R_-$ as V_H/I makes equation (3.1) identical to equation (2.31).

During operation, the magnet requires liquid helium and liquid nitrogen (each of which is contained in a separate dewar). There is an instrument that monitors the level of both cryogens. The magnet is automatically shut off when the level of liquid helium falls below 15%. The procedure for cooling the magnet is somewhat intricate. First, the liquid helium dewar must be precooled with liquid nitrogen. Then, this liquid nitrogen is transferred to the liquid nitrogen dewar. Finally, the liquid helium dewar must be filled with liquid helium. The cryogens gradually boil off, and as a result, must be refilled every few days during an experimental run. A large part of the cost of running this experiment comes from the cost of liquid helium.

A cylindrical furnace heats the sample. It consists of two semicircular ceramic

elements that are contained inside a steel tube. It is located at the bottom of the cylindrical bore. It has a circular hole in the center into which the base of the cryostat fits. The furnace is water cooled because otherwise the outside would get very hot and potentially damage the magnet. During initial tests without water cooling, the outside was about 100°C when the inside was about 200°C. With the water cooling in place, the furnace can be safely operated to temperatures of about 550°C without any detrimental effects to the magnet. See figure 3.2 for a picture of the furnace.

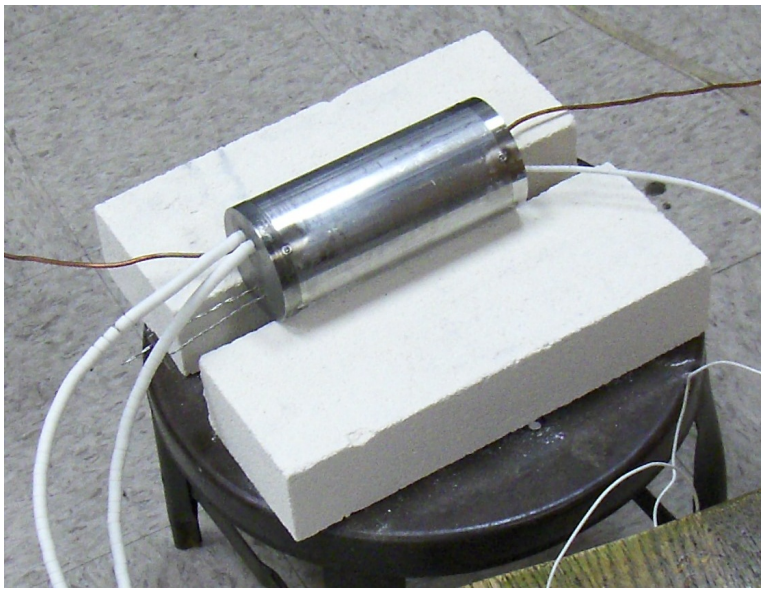

Figure 3.2: A side view of the furnace. Copper tubes carry water which cools the furnace. The wires covered with ceramic beads (on the left) carry current used to heat the furnace. The cryostat would enter from the right and rest inside the furnace. In the actual experiment, the furnace is upright.

The temperature of the furnace is regulated by a temperature controller, which is a Barber-Coleman model 2404. This temperature controller allows one to program multiple stages of heating, cooling, and dwelling at a constant temperature, as well as control the rate at which the temperature is increased. The temperature controller operates essentially as a feedback loop. The temperature at the sample is measured with a type K (chromel-alumel) thermocouple which sits in the ceramic platform next

to the sample. The measured temperature is compared with the target temperature. The temperature controller then adjusts the current that is being supplied to the furnace to bring the target temperature as close to the temperature inside the furnace as possible. Since data must be taken manually in this experiment, the temperature controller is usually reprogramed after each data acquisition. Data is usually acquired every 25 or 50°C, and the temperature is usually increased by about 4 or 5 degrees/minute. Since the temperature controller cannot supply sufficient current to the furnace, a solid state relay is used to actually supply the current–the temperature controller tells the relay how much current to source. There is a switch in the temperature control circuit which allows the temperature controller and relay to be disconnected from the furnace–this prevents from unintentionally heating the furnace when the experiment is not in use.

The sample sits on a ceramic platform at the base of a cryostat which fits into the furnace. The cryostat rests on the top of the magnet enclosure. See figures 3.3 and 3.4 for pictures of the cryostat. To prevent oxidation of the sample, the sample is enclosed in a quartz tube and is surrounded by about 1 atm of argon. There are valves at the top of the cryostat which allow air to be pumped out of the tube and argon to be pumped in, and there are tubes leading down the cryostat to the chamber in which the sample is contained. The quartz tube is connected to the cryostat via an o-ring and two semi-circular steel pieces. Initially, there was some concern that the tube was not being sealed sufficiently well; however, it does seem that the argon has a positive effect, as the sample looks much more oxidized after measurements in which no argon is used than in measurements in which argon is used.

The layout of the ceramic platform for the Hall coefficient experiment can be seen in figure 3.5. The sample is held in place by mechanical contacts. This poses

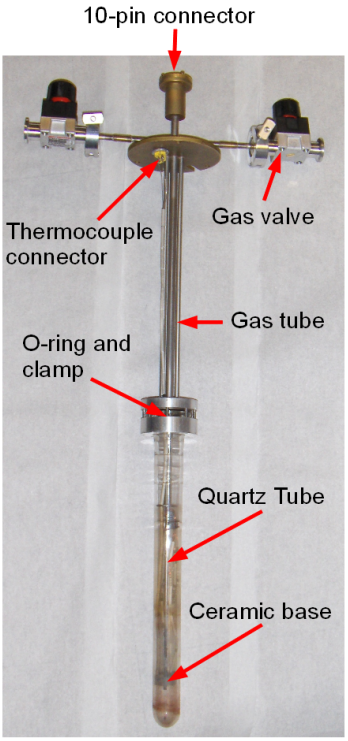

Figure 3.3: The cryostat which holds the sample.

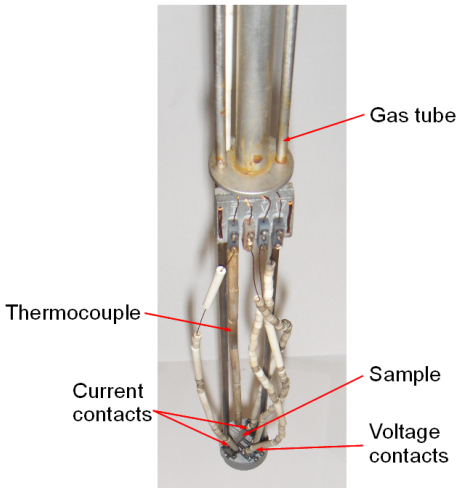

Figure 3.4: The bottom of the cryostat.

some difficulties, as many samples that are measured are very brittle and easily crack. Sometimes they crack while being set into place, and other times they crack because of thermal expansion of the sample and mechanical contacts. The current is distributed over the cross sectional area of the sample. A thin sheet of grafoil is inserted between the steel blocks and the sample (see figure 3.5). The grafoil sheet allows for a better electrical contact. By squeezing the sample, it also provides a better mechanical contact. The Hall voltage is measured between two point contacts, one of which is stationary and the other which is a screw with a very sharp tip. Each of the four contacts with the sample (the two current leads and the two Hall voltage probes) has a wire leading from it. These wires lead to a 10-pin connector at the top of the cryostat which mates with a cable that goes to the AC bridge.

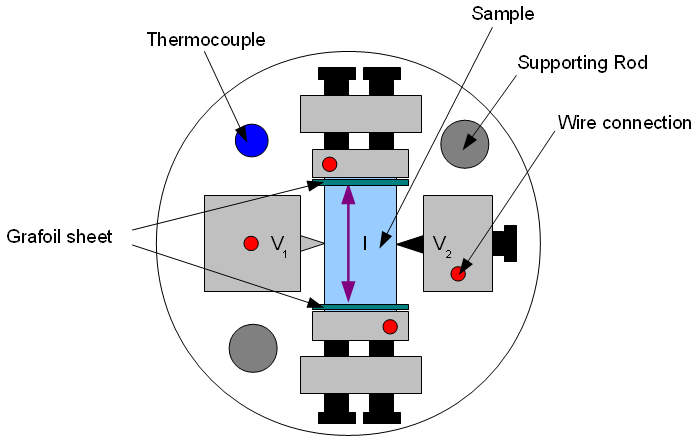

Figure 3.5: The layout of the ceramic platform for the Hall coefficient experiment. The red circles indicate the locations of the wires that lead to the AC Bridge. The thermocouple rests in a small hole next to the sample. One of the voltage contacts is fixed in place. The other three contacts can be adjusted with screws to fit the sample. The direction of current flow is indicated by the purple arrow.

3.3 Hall Coefficient Data

The high temperature Hall coefficient experiment has been quite successful since its completion, and over 100 samples have been measured with the setup. Most of the data that is presented below has been published in journal articles that survey various classes of thermoelectrics. As a result, comprehensive data on other thermoelectric properties of these materials is also readily available. While many classes of materials have been measured using the high temperature Hall effect experiment, I will focus on materials composed of lead telluride with some dopants added. Often, several samples were measured which differed only in the concentration of a particular dopant.

Most of my work on this project was done on the design and setup of the experiment. I have also assisted with some of the Hall effect measurements. It should be noted that some of the data that is presented in the following sections was taken by

others in the lab, and much of the analysis is derived from articles that the group has published. The main purpose of this section is to illustrate how the Hall coefficient is related to other thermoelectric properties and how it can provide useful information about a material.

3.3.1 Errors in Measuring the Hall Coefficient

The method used to measure the Hall coefficient involves measuring a very small resistance. For a typical sample with $n = 10^{20}$ cm^{-3}, a thickness of 2 mm, and a magnetic field of 1 T, the Hall resistance (see equation (3.1)) is about 30 $\mu\Omega$. The AC bridge uses a current on the order of 10 mA. Thus, by equation (2.31), $V_H \approx 300$ nV. Thus to achieve a 1% fractional uncertainty, the resolution must be on the order of 1 nV. This calculation emphasizes that the measurements being made are not trivial. The AC bridge described in the last section has the required precision.

An inspection of equation (3.1) shows that uncertainties in the resistance measurement, magnetic field magnitude, and thickness of the sample contribute to an uncertainty in the measured value of the Hall coefficient. Assuming the errors are Gaussian and independent,

$$\left(\frac{\sigma_{R_H}}{R_H}\right)^2 = \left(\frac{\sigma_{\Delta R}}{\Delta R}\right)^2 + \left(\frac{\sigma_t}{t}\right)^2 + \left(\frac{\sigma_B}{B}\right)^2 \tag{3.2}$$

where $\Delta R = R_+ - R_-$. The thickness t is measured with a micrometer, and the uncertainty is about 1%. The magnetic field is read out by the magnet power supply; however, from the specifications, we can assume that $\sigma_B/B << 0.01$ [6]. The major source of uncertainty is the resistance measurement, which has a fractional uncertainty in the range 1-10 % depending on the sample measured, but it is usually around 1-2 %. The uncertainty in the resistance measurement arises from fluctuations in the resistance reading from the AC bridge and in drifts in the resistance

reading that are relatively constant over the time required for a measurement. Both of these effects become more of a problem at high temperatures. Two main reasons why this might occur are chemical reactions between the sample and the electrical contacts that could occur at higher temperatures and Johnson (thermal) noise. Johnson noise is the result of thermally induced motions of charged particles, and the power of the Johnson noise is proportional to temperature [8]. Combining all of the errors, a conservative estimate of the fractional error is $\sigma R_H/R_H \leq 5\%$. To avoid cluttering the plots, error bars are not included.

3.3.2 PbTe+8% PbS

This sample was interesting because measurements were done on two samples, one which was annealed and the other which was not. The Hall coefficient as a function of temperature can be seen in figure 3.6. Notice that the Hall coefficient is essentially the same for both samples above about 600 K. At lower temperatures, the Hall coefficient differs significantly between the two samples. This data shows that annealing the sample (which occurs by heating the sample) has a major effect on the Hall coefficient and carrier density–the carrier density is higher (the Hall coefficient is smaller) when the sample is annealed. If the unannealed sample were measured again, its Hall coefficient would roughly follow that of the annealed sample, since measuring the unannealed sample from room temperature to about 800 K effectively anneals the sample.

3.3.3 PbTe-Si Eutectic Composites

The materials in this family have the general formula PbTe+Si(8%)+x% PbI_2 and are described in detail in Ref. [1]. PbI_2 is an n-type dopant that can be used to precisely control the thermoelectric properties. PbTe is usually quite brittle, but the

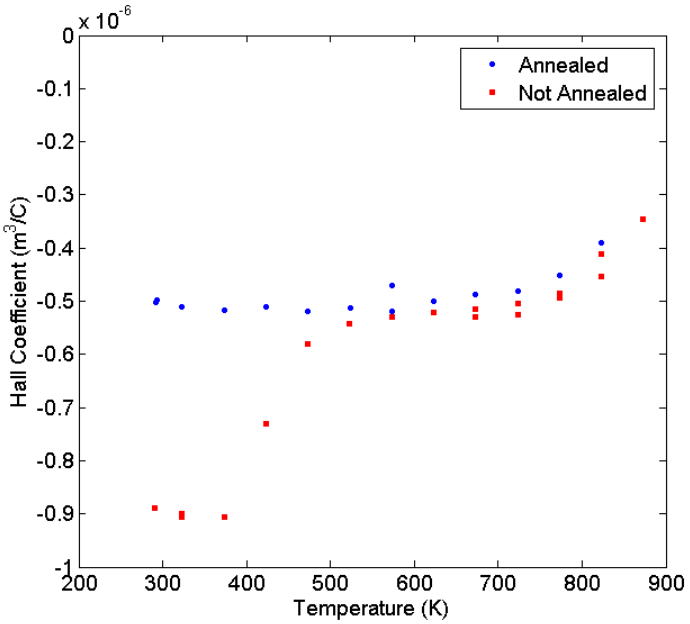

Figure 3.6: Hall coefficient data for PbTe+8% PbS

PbTe-Si system has much better mechanical properties, which is mainly due to the fact that they have a microstructure that makes it difficult for cracks to propagate [1]. In addition to improving the mechanical properties, another nice feature of doping with PbI_2 is that it does not significantly increase the thermal conductivity, which is crucial to maintaining a high figure of merit (recall, the figure of merit is inversely proportional to the thermal conductivity). In fact, it has been possible to reduce the thermal conductivity in some of these eutectic materials [1].

A eutectic material is a material that has a composition such that it solidifies at a lower temperature than any other composition. For the system y PbTe+x Si, it was found that the eutectic system occurs when $y = 0.92$ and $x = 0.08$, and the eutectic point occurs at a temperature about 900°C [1].

The concentration of PbI_2 allows for a fine tuning of the carrier concentration [1]. A graph of the Hall coefficient as a function of temperature and PbI_2 concentration

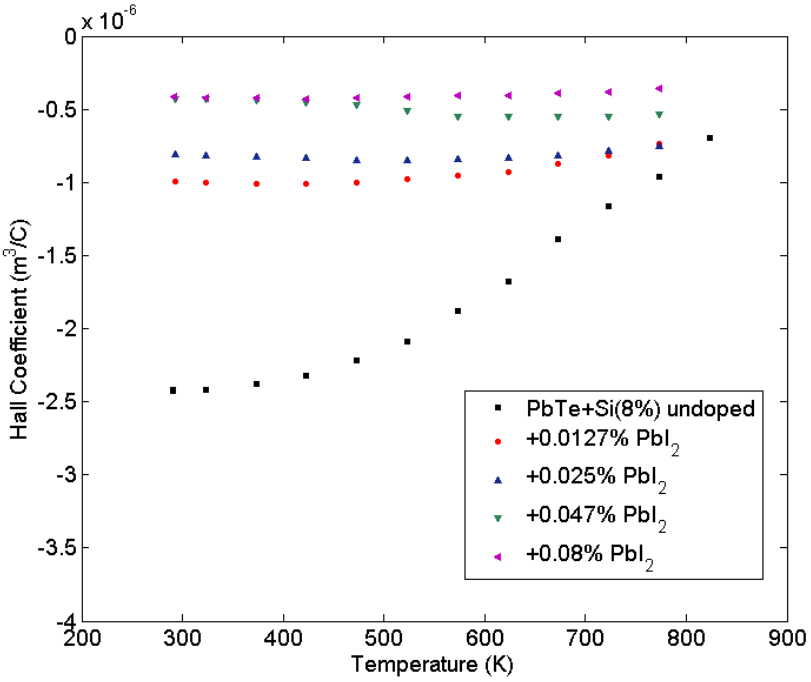

Figure 3.7: Hall coefficient data for PbTe+Si(8%)+x% PbI_2. This data is used in Ref. [1].

can be seen in figure 3.7. The magnitude of the Hall coefficient generally decreases as the concentration of PbI_2 increases, which means that the carrier concentration increases as the concentration of PbI_2 increases. This causes the electrical conductivity to increase with increasing PbI_2 concentration, which is confirmed by the electrical conductivity data, which can be seen in figure 3.8.

Another point to note about the Hall coefficient is that the value is relatively stable over the measured temperature range in the doped samples, while the magnitude decreases significantly with increasing temperature for the undoped sample. The reason for the decrease in R_H for the undoped sample is an increase in carrier excitations at high temperature [1].

These samples achieve a modest value of ZT. The maximum value was found to be about 0.9 at 660 K for the sample with 0.047% PbI_2. The data suggests that ZT should become greater than 1 for temperatures around 750-800 K [1]. A plot of the

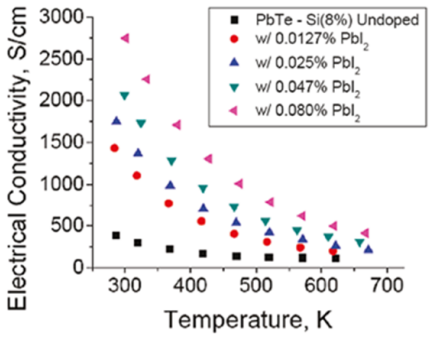

Figure 3.8: The electrical conductivity of PbTe+Si(8%)+x% PbI_2. Taken from Ref. [1].

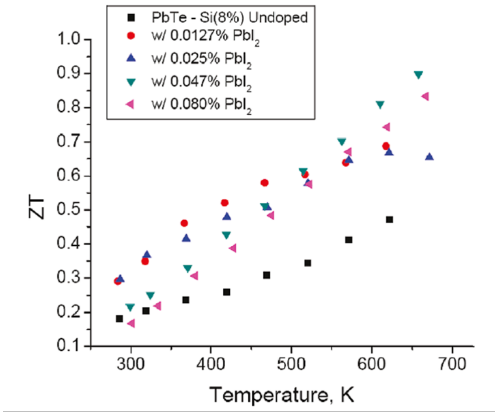

Figure 3.9: ZT for PbTe+Si(8%)+x% PbI_2. Taken from Ref. [1].

figure of merit as a function of temperature can be seen in figure 3.9.

The performance of this class of materials is promising. In addition to the relatively high values of ZT that were achieved, these materials are easy to produce, and they have desirable mechanical properties. As a result, they might be used in the future to fabricate thermoelectric modules [1].

3.3.4 $NaPb_{18-x}Sn_xMTe_{20}$ with M = Sb or Bi

Materials with the composition $NaPb_{18-x}Sn_xMTe_{20}$ (M = Sb or Bi) have the same structure as NaCl. These are p-type materials, and the fraction of Sn greatly affects the physical and thermoelectric properties [9]. The Hall coefficient for $NaPb_{15}Sn_3BiTe_{20}$ and $NaPb_{13}Sn_5SbTe_{20}$ is shown in figure 3.10. These two materials have quite small Hall coefficients; as a result, their carrier concentrations are quite large, around $10^{20}/cm^3$. Notice that the Hall coefficient is positive, which verifies that the materials are p-type.

The electrical conductivity as a function of temperature can be seen in figures 3.11 and 3.12. Combining the Hall coefficient measurement with the conductivity measurement, one finds that the mobility decreases from about 54 $cm^2/(V \cdot s)$ at room

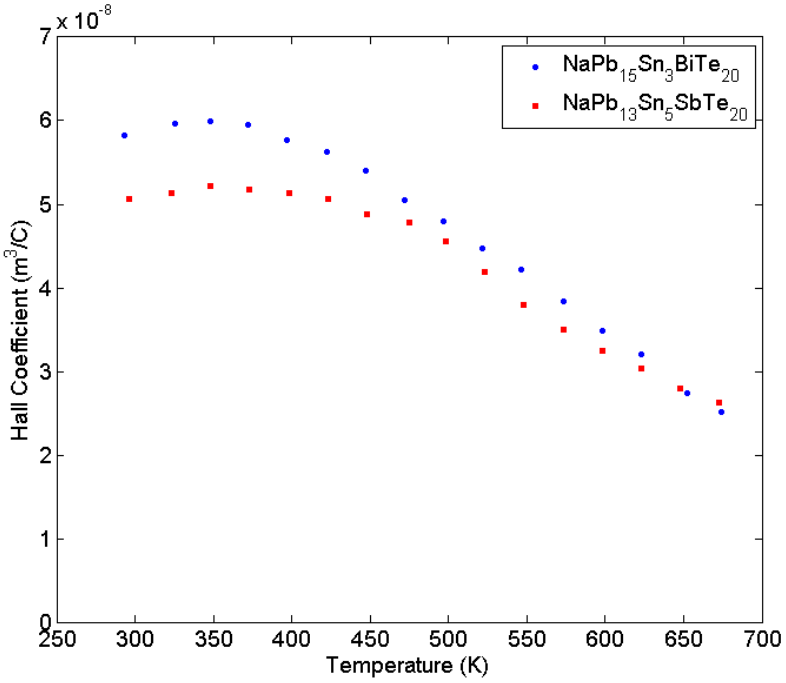

Figure 3.10: Hall coefficient data for $NaPb_{15}Sn_3BiTe_{20}$ and $NaPb_{13}Sn_5SbTe_{20}$. This data is used in Ref. [9].

temperature to about 7 $cm^2/(V \cdot s)$ for $NaPb_{13}Sn_5SbTe_{20}$. A similar decrease occurs for $NaPb_{15}Sn_3BiTe_{20}$. This small value for the mobility at high temperatures can be explained by the high carrier concentration and strong scattering of charge carriers on lattice vibrations (phonons) [9].

3.3.5 $AgPb_mLaTe_{m+2}$

Comprehensive measurements were taken on the materials $AgPb_mLaTe_{m+2}$ [10]. Data for the Hall coefficient is shown in figure 3.13, while data for electrical conductivity is shown in figure 3.14. The Hall coefficient is negative, which is indicative of n-type conduction.

These samples show interesting general trends, such as an increasing electrical conductivity for larger values of m (although the materials with $m = 18$ and $m = 25$ depart from this trend). The Seebeck coefficient is plotted in figure 3.15. A com-

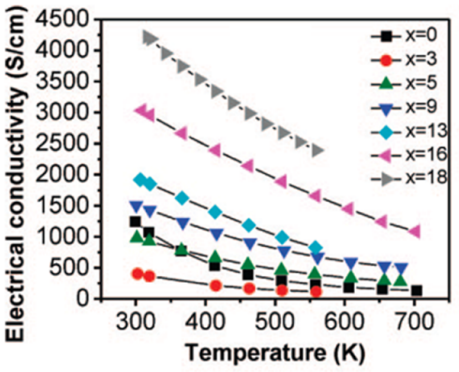

Figure 3.11: The electrical conductivity of $NaPb_{18-x}Sn_xSbTe_{20}$. Taken from Ref. [9].

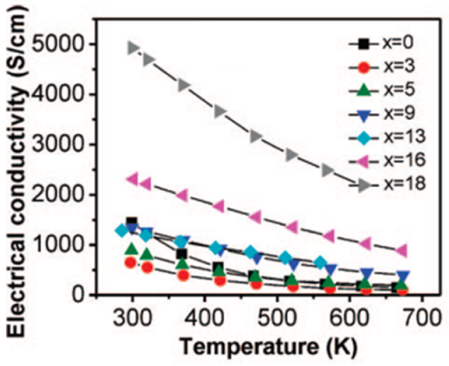

Figure 3.12: The electrical conductivity of $NaPb_{18-x}Sn_xBiTe_{20}$. Taken from Ref. [9].

parison of figures 3.13 and 3.15 shows a general trend of thermoelectrics–a higher carrier concentration (a smaller Hall coefficient) results in a smaller Seebeck coefficient magnitude [10]. $AgPb_{35}LaTe_{37}$ has the smallest Hall coefficient and also the smallest Seebeck coefficient magnitude over the entire temperature range measured.

3.3.6 PbTe with La and Ag

This class of materials consisted of lead telluride doped with lanthanum and codoped with silver and lanthanum [11]. La acts an electron donor; as a result, the electrical conductivity is much greater than in pure PbTe, and the carrier concentration is much higher [11]. A plot of the Hall coefficient for several different compositions can be seen in figure 3.17, while the electrical conductivity as a function of temperature is plotted in figure 3.18. The electrical conductivity of pure PbTe at room temperature is about 400 S/cm, which is much less that for the doped samples (this can clearly be seen in the left plot in figure 3.18) [11]. The small Hall coefficient for $Pb_{0.95}La_{0.05}Te$ compared with the other materials (including $Pb_{0.99}La_{0.01}Te$) confirms that the addition of La increases the carrier concentration.

On the other hand, silver is an electron acceptor, so Ag doping should have the

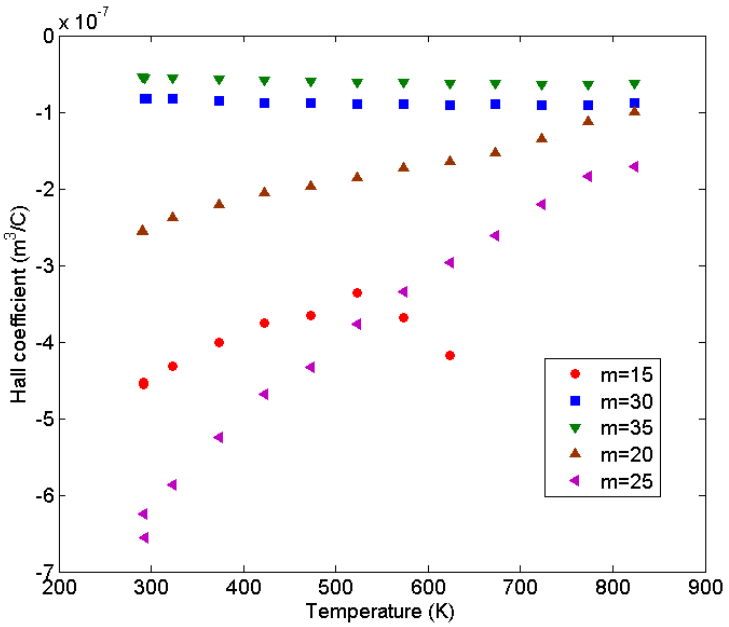

Figure 3.13: The Hall coefficient vs. temperature for $AgPb_mLaTe_{m+2}$. This data is used in Ref. [10].

opposite effect [11]. This is indeed the case, as can be seen in figure 3.17, where the Hall coefficient for $Ag_{0.05}Pb_{0.99}La_{0.01}Te$ and $Ag_{0.1}Pb_{0.99}La_{0.01}Te$ is greater than the Hall coefficient for the samples with no Ag. The figure of merit ZT is higher for the Ag doped compounds, as can be seen in figure 3.16. This makes sense based on the fact that the Seebeck coefficient is larger when the carrier concentration is smaller (see figure 3.19). The thermal conductivity of the Ag/La doped samples is slightly smaller than that of the samples that were doped only with La [11]. These two properties result in a higher ZT for the Ag/La codoped materials.

3.4 Future Work

The high temperature Hall effect experiment is regularly used and has become a standard measurement performed on most samples in the lab. It works very well, but there are a few possible improvements which could be made. For example, the current furnace can only be operated to about 550°C. By replacing this furnace with

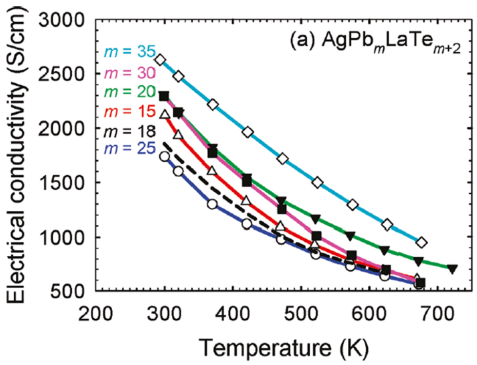

Figure 3.14: The electrical conductivity vs. temperature for $AgPb_mLaTe_{m+2}$. Taken from Ref. [10].

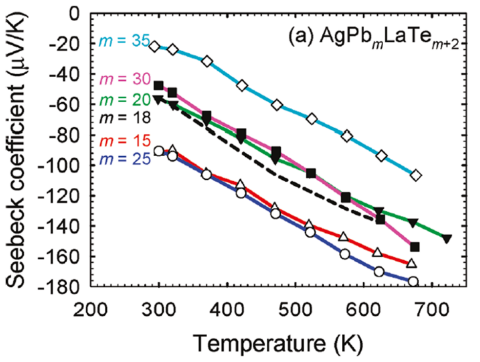

Figure 3.15: The Seebeck coefficient for $AgPb_mLaTe_{m+2}$. Taken from Ref. [10].

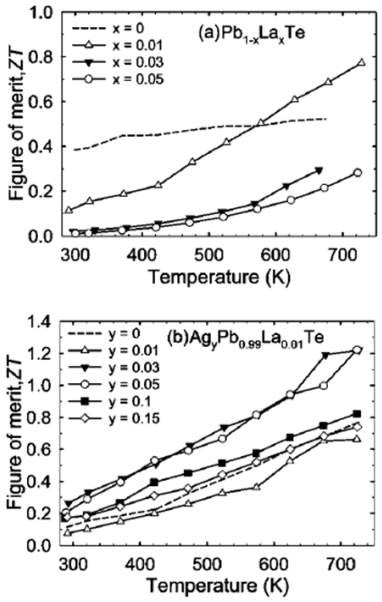

Figure 3.16: ZT for La doped and La/Ag codoped PbTe. Taken from Ref. [11].

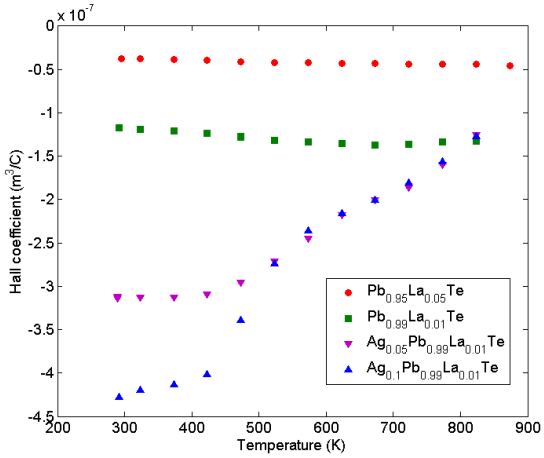

Figure 3.17: The Hall coefficient vs. temperature for La doped and La/Ag codoped PbTe. This data is used in Ref. [11].

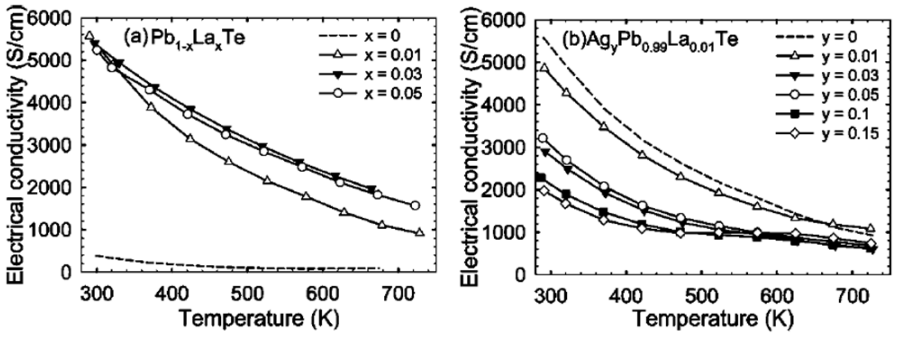

Figure 3.18: The electrical conductivity of La doped and La/Ag codoped PbTe. Taken from Ref. [11].

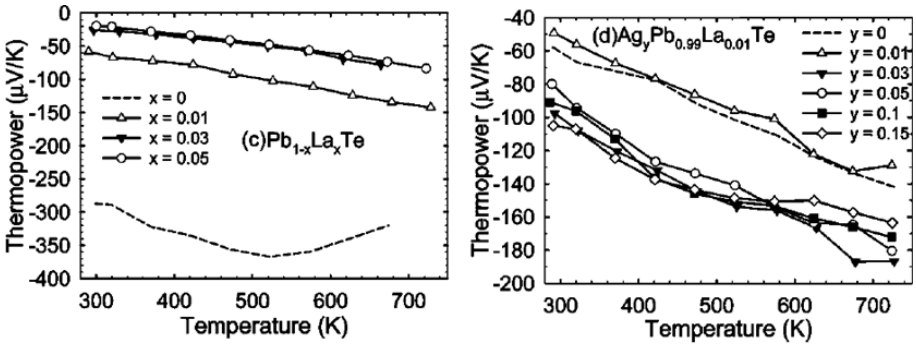

Figure 3.19: The Seebeck coefficient of La doped and La/Ag codoped PbTe. Taken from Ref. [11].

a larger version and implementing a better water cooling system to cool it, this range might be extended. Another inconvenient feature of the experiment is that the data must be taken manually; thus, someone must always be present while the experiment is running. It should be possible in principle to design an automated system to take the data. However, the equipment used for the measurements is quite old, and drivers for LabVIEW or some other program would have to be obtained or written.

CHAPTER IV

Conductivity Experiment and LabVIEW Programming

After the high temperature Hall effect experiment was up and running, I began to work on the construction of another experimental setup that utilizes the cylindrical geometry offered by the superconducting magnet. This experiment measures electrical conductivity, and unlike the Hall coefficient experiment, the data acquisition is done via computer control.

4.1 Motivation

There is a homemade experimental setup in the lab which measures the Seebeck coefficient and electrical conductivity. However, there was a desire to build a second experiment to measure electrical conductivity. There were two main motivations for building the new setup: to be able to check the values measured from the original setup, and to hopefully improve the measurement by using an AC measurement instead of a DC measurement. An AC measurement of electrical conductivity is inherently more accurate than a DC measurement. This is because any temperature difference between the two contacts from which a voltage measurement is made will create a Seebeck voltage, which will either be added to or subtracted from the reading, leading to errors. By using an AC measurement, this effect is avoided, because the errors cancel when the current changes polarity [3].

4.2 Experimental Setup

The cylindrical geometry of the superconducting magnet with the furnace in place provides a suitable location in which to perform the conductivity experiment. By constructing a new ceramic base, the same cryostat used for the Hall coefficient experiment can be used. The sample mount can be seen in figure 4.1. To measure conductivity, an AC bridge is used. The voltage along the length of the sample is measured (this is simply $V_1 - V_2$ in figure 4.1), and an average over time of the ratio of the voltage measurements to current gives a resistance measurement. This resistance measurement is then converted to conductivity by the equation

$$\sigma = \frac{L}{AR} \tag{4.1}$$

where L is the distance between the two voltage contacts, A is the cross sectional area of the sample, and R is the resistance measurement. Several assumptions are being made in equation (4.1), namely that the current is uniformly distributed over the cross sectional area of the sample and that Ohm's law is valid. The voltage contacts leave indentations on the sample. The length L can be measured fairly precisely by measuring the distance between these indentations using a microscope. The other dimensions are measured with a micrometer.

A LabVIEW VI was written to control the data acquisition for this experiment. The data is written to a text file where it can then be imported into other software for further analysis. The front panel is shown in figure 4.2, and the block diagram is shown in figure 4.3. The front panel allows the user to start and stop measurements, choose the file in which the data will be saved, and calibrate the AC bridge and the voltmeter used to measure temperature. This program was designed to be very user

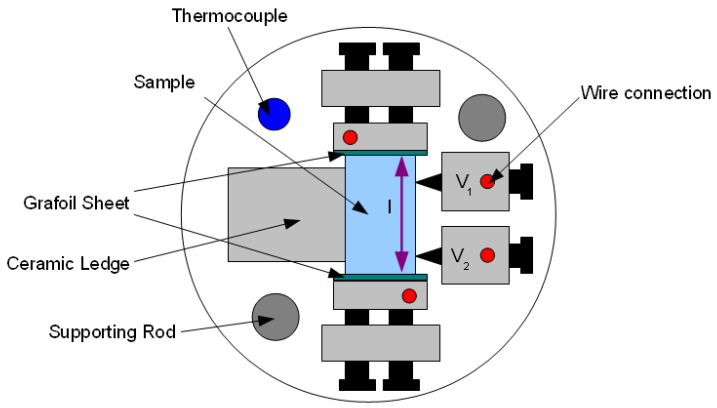

Figure 4.1: The layout of the ceramic platform for the conductivity experiment. The layout is very similar to that for the high temperature Hall coefficient experiment, except that here the voltages are both measured from the same side of the sample. The left side of the sample rests against a ceramic ledge.

friendly, and in principle the program can be running all the time.

The temperature controller does not have a standard protocol for communication with LabVIEW; thus, a multimeter (Keithley 2120) is used to measure the temperature and transfer the temperature readings to the computer. This multimeter has the capability of measuring temperature directly from many standard thermocouple types. The multimeter can be calibrated by setting the thermocouple type and setting the reference temperature junction (which is room temperature in this case). By calibrating the multimeter, the temperature reading that it gives and the temperature reading from the temperature controller usually differ by less than 1 Kelvin at all times. Since the computer does not actually control the temperature controller, the temperature controller must be set manually; however, it only needs to be programmed once. This is a desirable feature to the experiment, because it means that the experiment does not need to be attended while it is running. A new AC bridge (Lakeshore 370) was purchased for this experiment. This is a much more modern design than the AC bridge used in the Hall coefficient experiment, and it

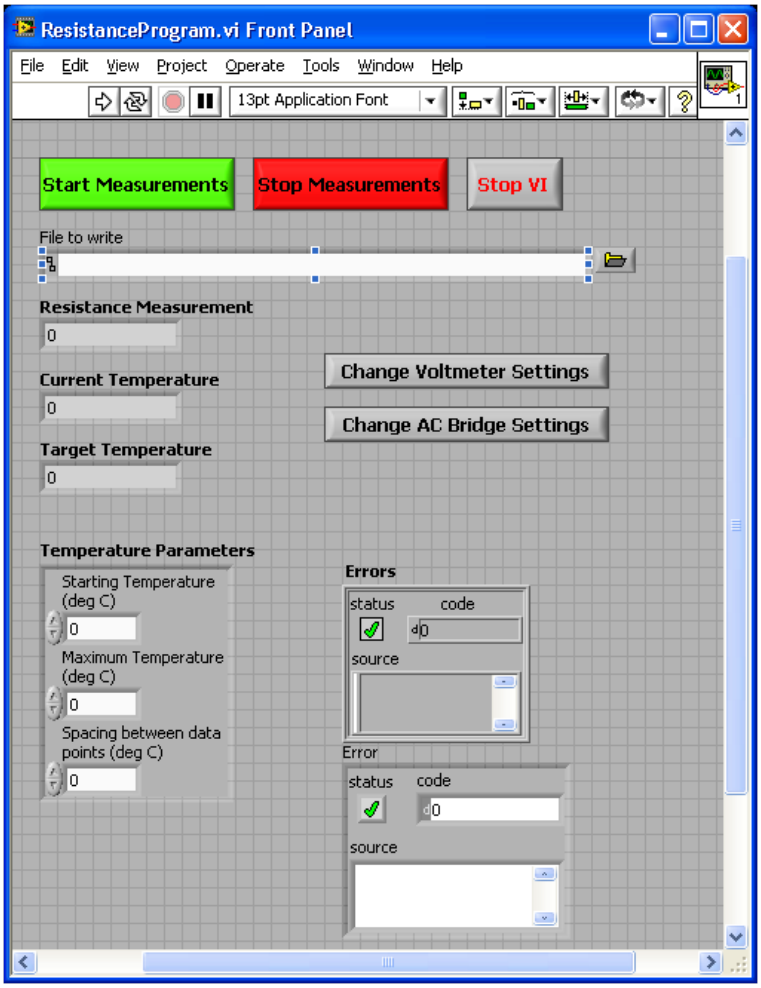

Figure 4.2: The front panel of the conductivity VI

was very straightforward to write LabVIEW drivers for it.

The user sets the starting temperature (which is usually 25°C), the maximum temperature (which is usually around 500°C), and the temperature interval between data points (which is typically 25°C). The target temperature is initially set equal to the starting temperature. The program measures the temperature every 10 seconds. When the measured temperature exceeds the target temperature, a resistivity measurement is taken, and the target temperature is increased by the temperature spacing. Once the maximum temperature is attained, the target temperature begins to decrease, and the entire process repeats going down in temperature.

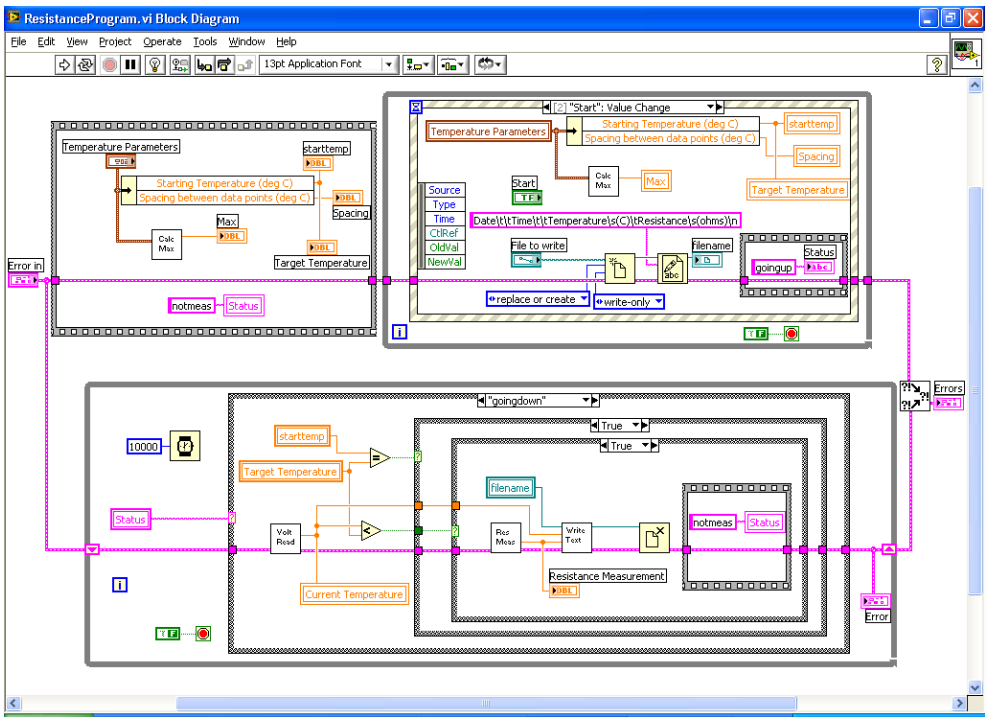

Figure 4.3: The block diagram of the conductivity VI. The loop in the upper left initializes the program, the loop in the upper right utilizes LabVIEW's event structure, and the bottom loop actually carries out the measurements and writes the data to a text file.

The VI uses some of LabVIEW's advanced features to streamline the operation. Most of the controls on the front panel, such as the start and stop buttons and the calibration buttons, are controlled by an event structure. This means that the code associated with these icons only executes when these icons are clicked on.

4.3 Some Preliminary Results

As mentioned above, one of the main purposes of this new conductivity setup was to check the values measured on the original apparatus. As a result, the first samples measured on this new setup were samples that had previously been measured with the old setup. In the initial tests, the two experiments gave fairly consistent results. A plot comparing data taken for $Ba_{0.1}Yb_{0.1}In_{0.1}Ba_4Sb_{12}$ (which is a skutterudite) in both setups can be seen in figure 4.4.

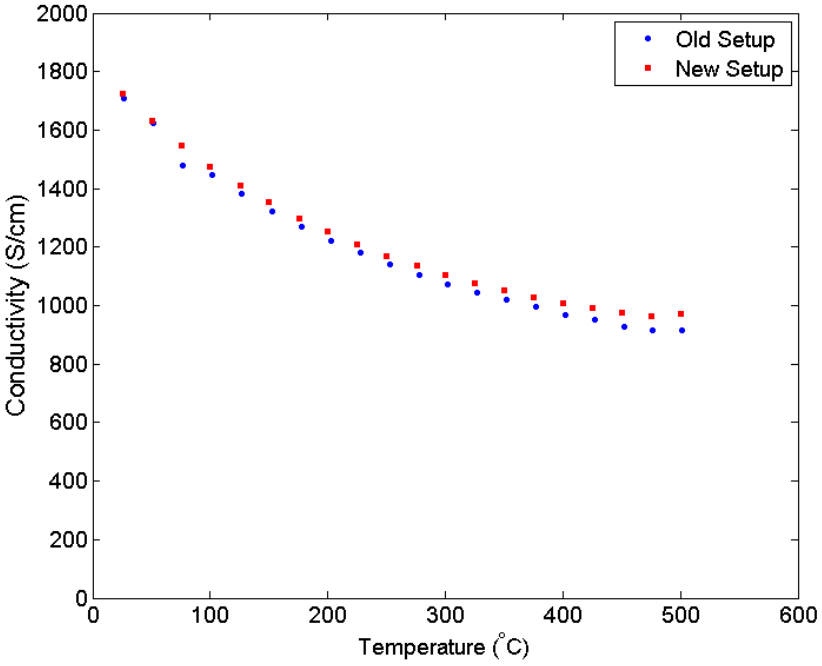

Figure 4.4: Comparison of the two conductivity setups. This data was taken for the material $Ba_{0.1}Yb_{0.1}In_{0.1}Ba_4Sb_{12}$, which is a skutterudite.

4.4 Other Projects

The experimental setup in the lab that measures electrical conductivity and the Seebeck coefficient is also operated by a LabVIEW VI. However, the VI was written several years ago, and it was not documented very well, so it was difficult to assess its performance. I spent some time isolating the part of the program that measures the Seebeck coefficient and made a new VI that behaves similarly to the conductivity VI that I wrote, except that it only measures the Seebeck coefficient. The structure and user interface is otherwise very similar. This program can be modified in several useful ways that will allow the measurement process to vary depending on the sample being measured. It allows the user to control how many measurements are carried out at each target temperature, and also control the duration of each measurement. It may be desirable to vary these parameters from one sample to another, and this

program provides an easy mechanism for doing so.

4.5 Further Work

The new conductivity experiment works quite well. In addition to providing a way to check the data measured on the other setup, it also gives the opportunity to measure more than one sample at the same time, which may be useful when there are many samples that need to be measured. Possible improvements to this setup include devising a way to control the temperature controller directly and installing a heater in the new setup, which would enable the Seebeck coefficient to be measured (this would give two experiments that would have the capability of measuring both electrical conductivity and the Seebeck coefficient).

CHAPTER V

Conclusion and Prospects for Further Work

While the figure of merit does not directly involve the Hall coefficient or carrier concentration, the quantities that it depends on (including electrical conductivity and the Seebeck coefficient) do depend on the carrier concentration. A lot of valuable information about a material can be obtained from a measurement of the Hall coefficient.

A measurement of the Hall coefficient at room temperature is rather routine. However, the experimental system described in this thesis is one of the only systems in the world capable of accurately measuring the Hall coefficient at high temperatures.

Novel thermoelectric materials have the potential to reduce the amount of wasted heat in many systems. This would reduce society's energy consumption and make industrial processes cleaner and more efficient. Right now, the field is at a stage where new materials are being produced and characterized. There is still a lot of progress that needs to be made in order to develop materials that can be used in practical situations; however, the study of thermoelectric materials is a very worthwhile endeavor. In addition to the potential practical applications of novel thermoelectrics, studying thermoelectrics is rewarding in its own right, as it increases our understanding of phenomena in solid state physics and physical chemistry.

PUBLICATIONS

Many of the measurements from the Hall coefficient experiment have been discussed in journal articles. I am coauthor on three articles, two which have already been published, and another which will be published soon. The citations are as follows:

- A. Guéguen, P. F. P. Poudeu, C. Li, S. Moses, C. Uher, J. He, V. Dravid, K. M. Paraskevopoulos, and M. G. Kanatzidis. Thermoelectric properties and nanostructuring in the p-type materials $NaPb_{18-x}Sn_xMTe_{20}$ (M= Sb, Bi). *Chemistry of Materials*, 21 (8): 1683-1694, 2009.
- K. Ahn, M. Han, D. Vermeulen, S. Moses, C. Uher, and M. Kanatzidis. The effect on thermoelectric properties of Cd substitution in PbTe. *Materials Research Society Symposium Proceedings*, 1166-N06-09, 2009.
- S. Girard, J. He, C. Li, S. Moses, G. Wang, C. Uher, D. Vinayak, and M. Kanatzidis. In situ nanostructure generation and evolution within a bulk thermoelectric material to reduce lattice thermal conductivity. *Nano Letters*, submitted.

BIBLIOGRAPHY

[1] J. R. Sootsman, J. He, V. P. Dravid, S. Ballikaya, D. Vermeulen, C. Uher, and M. G. Kanatzidis. Microstructure and thermoelectric properties of mechanically robust PbTe-Si eutectic composites. *Chemistry of Materials*, 22(3):869–875, 2010.

[2] H. J. Goldsmid. Conversion efficiency and figure-of-merit. In D. M. Rowe, editor, *CRC Handbook of Thermoelectrics*, pages 19–25. CRC Press, 1995.

[3] G. S. Nolas, J. Sharp, and H. J. Goldsmid. *Thermoelectrics: Basic Principles and New Materials Development*. Springer, Berlin, 2001.

[4] C. Kittel. *Introduction to Solid State Physics*. Wiley, New York, seventh edition, 1996.

[5] A. C. Melissinos. *Experiments in Modern Physics*. Academic Press, New York, first edition, 1966.

[6] *Superconducting Magnet System, Operator's Handbook*. Oxford Instruments, 1996.

[7] *User's Manual, Model 370 AC Resistance Bridge*. Lakeshore Cryotronics, Inc., Westerville, Ohio, 2008.

[8] *Low Level Measurements Handbook: Precision DC Current, Voltage, and Resistance Measurements*. Keithley, Cleveland, Ohio, sixth edition, 2004.

[9] A. Guéguen, P. F. P. Poudeu, C. Li, S. Moses, C. Uher, J. He, V. Dravid, K. M. Paraskevopoulos, and M. G. Kanatzidis. Thermoelectric properties and nanostructuring in the p-type materials $NaPb_{18-x}Sn_xMTe_{20}$ (M= Sb, Bi). *Chemistry of Materials*, 21(8):1683–1694, 2009.

[10] K. Ahn, C. Li, C. Uher, and M. G. Kanatzidis. Thermoelectric properties of the compounds $AgPb_mLaTe_{m+2}$. *Chemistry of Materials*, 22(3):876–882, 2010.

[11] K. Ahn, C. Li, C. Uher, and M. G. Kanatzidis. Improvement in the thermoelectric figure of merit by La/Ag cosubstitution in PbTe. *Chemistry of Materials*, 21(7):1361–1367, 2009.